

Solar cell efficiency tables (Version 60)

Martin A. Green¹  | Ewan D. Dunlop² | Jochen Hohl-Ebinger³ |
 Masahiro Yoshita⁴ | Nikos Kopidakis⁵ | Karsten Bothe⁶ | David Hinken⁶ |
 Michael Rauer³  | Xiaojing Hao¹

¹Australian Centre for Advanced Photovoltaics, School of Photovoltaic and Renewable Energy Engineering, University of New South Wales, Sydney, New South Wales, Australia

²European Commission – Joint Research Centre, Ispra, Varese, Italy

³Department of Characterisation and Simulation/CalLab Cells, Fraunhofer-Institute for Solar Energy Systems, Freiburg, Germany

⁴Renewable Energy Research Center (RENRC), National Institute of Advanced Industrial Science and Technology (AIST), Tsukuba, Ibaraki, Japan

⁵Solar Energy Research Facility, National Renewable Energy Laboratory, Golden, Colorado, USA

⁶Calibration and Test Center, Solar Cells Laboratory, Institute for Solar Energy ResearchGmbH (ISFH), Emmerthal, Germany

Correspondence

Martin A. Green, School of Photovoltaic and Renewable Energy Engineering, University of New South Wales, Sydney, NSW 2052, Australia.

Email: m.green@unsw.edu.au

Funding information

Ministry of International Trade and Industry (MITI); New Energy and Industrial Technology Development Organization; U.S. Department of Energy (Office of Science, Office of Basic Energy Sciences and Energy Efficiency and Renewable Energy, Solar Energy Technology Program), Grant/Award Number: DE-AC36-08-GO28308; Ministry of Economy, Trade and Industry (METI); Japanese New Energy and Industrial Technology Development Organisation (NEDO); Australian Renewable Energy Agency (ARENA)

Abstract

Consolidated tables showing an extensive listing of the highest independently confirmed efficiencies for solar cells and modules are presented. Guidelines for inclusion of results into these tables are outlined, and new entries since January 2022 are reviewed. An appendix describing temporary electrical contacting of large-area solar cells approaches and terminology is also included.

KEY WORDS

energy conversion efficiency, photovoltaic efficiency, solar cell efficiency

1 | INTRODUCTION

Since January 1993, *Progress in Photovoltaics* has published six monthly listings of the highest confirmed efficiencies for a range of photovoltaic cell and module technologies.^{1–3} By providing guidelines for inclusion of results into these tables, this not only provides an authoritative summary of the current state-of-the-art but also encourages researchers to seek independent confirmation of results and to report results on a standardised basis. In Version 33 of these tables,² results were updated to the new internationally accepted reference spectrum (International Electrotechnical Commission IEC 60904-3, Ed. 2, 2008).

The most important criterion for inclusion of results into the tables is that they must have been independently measured by a recognised test centre listed in an earlier issue³ (also see present Appendix B). A distinction is made between three different eligible definitions of cell area: total area, aperture area and designated illumination area, as defined in an earlier issue³ (note that, if masking is used, masks must have a simple aperture geometry, such as square, rectangular or circular—masks with multiple openings are not eligible). ‘Active area’ efficiencies are not included. There are also certain minimum values of the area sought for the different device types (above 0.05 cm² for a concentrator cell, 1 cm² for a one-sun cell, 800 cm² for a module and 200 cm² for a ‘submodule’).

In recent years, approaches for contacting large-area solar cells during measurement have become increasingly complex. Because there is no explicit standard for the design of solar cell contacting units, in Appendix A of this issue, we describe approaches for temporary electrical contacting of large-area solar cells with and without busbars. In order to enable comparability between different contacting approaches and to clarify the corresponding measurement conditions, an unambiguous denotation is introduced that will be used in future versions of these tables.

Table results are reported for cells and modules made from different semiconductors and for subcategories within each semiconductor grouping (e.g., crystalline, polycrystalline or directionally solidified and thin film). From Version 36 onwards, spectral response information is included (when possible) in the form of a plot of the external quantum efficiency (EQE) versus wavelength, either as absolute values or normalised to the peak measured value. Current–voltage (IV) curves have also been included where possible from Version 38 onwards. A graphical summary of progress over the 28 years during which the tables have been published is included in an earlier issue.³

Highest confirmed ‘one sun’ cell and module results are reported in Tables 1–4. Any changes in the tables from those previously published¹ are set in bold type. In most cases, a literature reference is provided that describes either the result reported, or a similar result (readers identifying improved references are welcome to submit to the lead author). Table 1 summarises the best-reported measurements for ‘one-sun’ (non-concentrator) single-junction cells and submodules.

Table 2 contains what might be described as ‘notable exceptions’ for ‘one-sun’ single-junction cells and submodules in the above category. While not conforming to the requirements to be recognised as a

class record, the devices in Table 2 have notable characteristics that will be of interest to sections of the photovoltaic community, with entries based on their significance and timeliness. To encourage discrimination, the table is limited to nominally 12 entries with the present authors having voted for their preferences for inclusion. Readers who have suggestions of notable exceptions for inclusion into this or subsequent tables are welcome to contact any of the authors with full details. Suggestions conforming to the guidelines will be included on the voting list for a future issue.

Table 3 was first introduced in Version 49 of these tables and summarises the growing number of cell and submodule results involving high efficiency, one-sun multiple-junction devices (previously reported in Table 1). Table 4 shows the best results for one-sun modules, both single and multiple junctions, while Table 5 shows the best results for concentrator cells and concentrator modules. A small number of ‘notable exceptions’ are also included in Tables 3–5.

2 | NEW RESULTS

Fifteen new results are reported in the present version of these tables. The first new result in Table 1 (‘one-sun cells and submodules’) is 19.8% efficiency for a large (665 cm²) CuIn_{1-x}Ga_xS₂ (CIGS) submodule fabricated by Avancis,¹² with the result confirmed by the US National Renewable Energy Laboratory (NREL). The submodule is only slightly too small for classification as a module (>800 cm²) and improves on the earlier 19.6% result from the same group. The second new result in Table 1 is 14.5% efficiency for a 19.3-cm² organic cell minimodule (a package of interconnected cells of area <200 cm²) fabricated by Zhejiang University (ZJU)²³ in conjunction with Microquanta and measured by the Japan Electrical Safety and Environment Technology Laboratories (JET), also improving on the team’s earlier 14.1% result. A third new result is 23.7% efficiency for a 1-cm² lead-halide perovskite solar cell fabricated by the University of Science and Technology of China, Hefei,¹⁸ and measured by the Chinese National PV Industry Measurement and Testing Center (NPVM).

There are three new results in Table 2 (one-sun ‘notable exceptions’). An efficiency of 25.3% is reported for a large-area (268-cm²) n-type silicon cell with polysilicon on thin-oxide rear contact (aka TOPCon) fabricated by JinkoSolar³⁴ and measured by the Institute für Solarenergieforschung (ISFH). Using the amorphous-silicon/silicon heterojunction (HJT) approach, an efficiency of 25.5% is reported for another large-area (274-cm²) gallium-doped p-type silicon cell fabricated by LONGi and again measured by ISFH. LONGi is reported as being convinced that this p-HJT cell route still has great potential for further development. An efficiency of 13.6% was measured for a 0.27-cm²Cu₂ZnSnS_xSe_{4-x} (CZTSSe) cell³⁷ by the Institute of Physics (IOP), Chinese Academy of Science (CAS) and measured by NPVM. The final new result in Table 2 is an efficiency of 25.7% measured for a small-area (0.096-cm²) perovskite cell fabricated by the Ulsan National Institute of Science and Technology (UNIST)³⁹ and measured by the Newport PV Laboratory, improving on UNIST’s earlier 25.5% result. For the latter two cells, cell area is too small for classification as

TABLE 1 Confirmed single-junction terrestrial cell and submodule efficiencies measured under the global AM1.5 spectrum (1000 W/m²) at 25°C (IEC 60904-3: 2008 or ASTM G-173-03 global)

Classification	Efficiency (%)	Area (cm ²)	V _{oc} (V)	J _{sc} (mA/cm ²)	Fill factor (%)	Test centre (date)	Description
Silicon							
Si (crystalline cell)	26.7 ± 0.5	79.0 (da)	0.738	42.65 ^a	84.9	AIST (3/17)	Kaneka, n-type rear IBC ⁴
Si (crystalline cell)	26.3 ± 0.4 ^b	274.3 (t)	0.7502	40.49 ^c	86.6	ISFH (9/21)	LONGi, n-type HJT ⁵
Si (DS wafer cell)	24.4 ± 0.3 ^b	267.5 (t)	0.7132	41.47 ^d	82.5	ISFH (8/20)	Jinko Solar, n-type
Si (thin transfer submodule)	21.2 ± 0.4	239.7 (ap)	0.687 ^e	38.50 ^{e,f}	80.3	NREL (4/14)	Solexel (35 μm thick) ⁶
Si (thin film minimodule)	10.5 ± 0.3	94.0 (ap)	0.492 ^e	29.7 ^{e,g}	72.1	FhG-ISE (8/07)	CSG Solar (<2 μm on glass) ⁷
III-V cells							
GaAs (thin film cell)	29.1 ± 0.6	0.998 (ap)	1.1272	29.78 ^h	86.7	FhG-ISE (10/18)	Alta Devices ⁸
GaAs (multicrystalline)	18.4 ± 0.5	4.011 (t)	0.994	23.2	79.7	NREL (11/95)	RTI, Ge substrate ⁹
InP (crystalline cell)	24.2 ± 0.5 ⁱ	1.008 (ap)	0.939	31.15 ^a	82.6	NREL (3/13)	NREL ¹⁰
Thin film chalcogenide							
CIGS (cell) (Cd-free)	23.35 ± 0.5	1.043 (da)	0.734	39.58 ^j	80.4	AIST (11/18)	Solar Frontier ¹¹
CIGSSe (submodule)	19.8 ± 0.3	665.4 (ap)	0.688	37.96 ^k	75.9	NREL (12/21)	Avancis, 110 cells ¹²
CdTe (cell)	21.0 ± 0.4	1.0623 (ap)	0.8759	30.25 ^f	79.4	Newport (8/14)	First Solar, on glass ¹³
CZTSSe (cell)	11.3 ± 0.3	1.1761 (da)	0.5333	33.57 ^h	63.0	Newport (10/18)	DGIST, Korea ¹⁴
CZTS (cell)	10.0 ± 0.2	1.113 (da)	0.7083	21.77 ^a	65.1	NREL (3/17)	UNSW ¹⁵
Amorphous/microcrystalline							
Si (amorphous cell)	10.2 ± 0.3 ^{l,i}	1.001 (da)	0.896	16.36 ^f	69.8	AIST (7/14)	AIST ¹⁶
Si (microcrystalline cell)	11.9 ± 0.3 ^j	1.044 (da)	0.550	29.72 ^a	75.0	AIST (2/17)	AIST ¹⁷
Perovskite							
Perovskite (cell)	23.7 ± 0.5 ^m	1.062 (da)	1.213	24.99 ^k	78.3	NPVM (5/22)	U.Sci.Tech., Hefei ¹⁸
Perovskite (minimodule)	21.4 ± 0.4 ^m	19.32 (da)	1.149 ^e	23.41 ^{e,b}	79.6	JET (10/21)	Microquanta, 7 cells ¹⁹
Dye sensitised							
Dye (cell)	11.9 ± 0.4 ⁿ	1.005 (da)	0.744	22.47 ^o	71.2	AIST (9/12)	Sharp ^{20,21}
Dye (minimodule)	10.7 ± 0.4 ⁿ	26.55 (da)	0.754 ^e	20.19 ^{e,p}	69.9	AIST (2/15)	Sharp, 7 serial cells ^{20,21}
Dye (submodule)	8.8 ± 0.3 ⁿ	398.8 (da)	0.697 ^e	18.42 ^{e,q}	68.7	AIST (9/12)	Sharp, 26 serial cells ^{20,21}
Organic							
Organic (cell)	15.2 ± 0.2 ^{j,r}	1.015 (da)	0.8467	24.24 ^d	74.3	FhG-ISE (10/20)	Fraunhofer ISE ²²
Organic (minimodule)	14.5 ± 0.3 ^r	19.31(da)	0.8518 ^e	23.51 ^{e,k}	72.5	JET (12/21)	ZJU/Microquanta, 7 cells ²³
Organic (submodule)	11.7 ± 0.2 ^r	203.98 (da)	0.8177 ^e	20.68 ^{e,s}	69.3	FhG-ISE (10/19)	ZAE Bayern, 33 cells ²⁴

Abbreviations: (ap), aperture area; (da), designated illumination area; (t), total area; AIST, Japanese National Institute of Advanced Industrial Science and Technology; a-Si, amorphous silicon/hydrogen alloy; CIGS, CuIn_{1-y}Ga_ySe₂; CZTS, Cu₂ZnSnS₄; CZTSSe, Cu₂ZnSnS_{4-y}Se_y; DS, directionally solidified (including mono cast and multicrystalline); FhG-ISE, Fraunhofer Institut für Solare Energiesysteme; nc-Si, nanocrystalline or microcrystalline silicon.

^aSpectral response and current–voltage curve reported in Version 50 of these tables.

^bContacting: Front: 9BB, busbar resistance neglecting; Rear: 9BB, full area contacting, highly reflective chuck.

^cSpectral response and current–voltage curve reported in Version 59 of these tables.

^dSpectral response and current–voltage curve reported in Version 57 of these tables.

^eReported on a ‘per cell’ basis.

^fSpectral responses and current–voltage curve reported in Version 45 of these tables.

^gRecalibrated from original measurement.

^hSpectral response and current–voltage curve reported in Version 53 of these tables.

ⁱNot measured at an external laboratory.

^jSpectral response and current–voltage curve reported in Version 54 of these tables.

^kSpectral response and current–voltage curve reported in present version of these tables.

^lStabilised by 1000-h exposure to 1 sun light at 50°C.

^mInitial performance. Han et al.²⁵ and Yang and You²⁶ review the stability of similar devices.

ⁿInitial efficiency. Krašovec et al.²⁷ review the stability of similar devices.

^oSpectral response and current–voltage curve reported in Version 41 of these tables.

^pSpectral response and current–voltage curve reported in Version 46 of these tables.

^qSpectral response and current–voltage curve reported in Version 43 of these tables.

^rInitial performance. Tanenbaum et al.²⁸ and Krebs²⁹ review the stability of similar devices.

^sSpectral response and current–voltage curve reported in Version 55 of these tables.

TABLE 2 ‘Notable exceptions’ for single-junction cells and submodules: ‘Top dozen’ confirmed results, not class records, measured under the global AM1.5 spectrum (1000 W m⁻²) at 25°C (IEC 60904-3: 2008 or ASTM G-173-03 global)

Classification	Efficiency (%)	Area (cm ²)	V _{oc} (V)	J _{sc} (mA/cm ²)	Fill factor (%)	Test centre (date)	Description
<u>Cells (silicon)</u>							
Si (crystalline)	25.0 ± 0.5	4.00 (da)	0.706	42.7 ^a	82.8	Sandia (3/99)	UNSW, p-type PERC ³⁰
Si (crystalline)	25.8 ± 0.5 ^b	4.008 (da)	0.7241	42.87 ^c	83.1	FhG-ISE (7/17)	FhG-ISE, n-type TOPCon ³¹
Si (crystalline)	26.0 ± 0.5 ^b	4.015 (da)	0.7323	42.05 ^d	84.3	FhG-ISE (11/19)	FhG-ISE, p-type TOPCon
Si (crystalline)	26.1 ± 0.3 ^b	3.9857 (da)	0.7266	42.62 ^e	84.3	ISFH (2/18)	ISFH, p-type rear IBC ³²
Si (large crystalline)	24.0 ± 0.3 ^f	244.59 (t)	0.6940	41.58 ^g	83.3	ISFH (7/19)	LONGi, p-type PERC ³³
Si (large crystalline)	25.3 ± 0.4 ^h	268.0 (t)	0.7214	42.07 ⁱ	83.4	ISFH (11/21)	Jinko, n-type TOPCon ³⁴
Si (large crystalline)	25.5 ± 0.4 ^j	274.3 (t)	0.7476	40.66 ⁱ	83.8	ISFH (11/21)	LONGi, p-type HJT
Si (large crystalline)	26.6 ± 0.5	179.74 (da)	0.7403	42.5 ^k	84.7	FhG-ISE (11/16)	Kaneka, n-type rear IBC ⁴
<u>Cells (III-V)</u>							
GalnP	22.0 ± 0.3 ^b	0.2502 (ap)	1.4695	16.63 ^l	90.2	NREL (1/19)	NREL, rear HJ, strained AlInP ³⁵
<u>Cells (chalcogenide)</u>							
CdTe (thin-film)	22.1 ± 0.5	0.4798 (da)	0.8872	31.69 ^m	78.5	Newport (11/15)	First Solar on glass ³⁶
CZTSSe (thin-film)	13.6 ± 0.3	0.2661 (ap)	0.5375	36.18 ⁱ	69.8	NPVM (5/22)	IOP, CAS ³⁷
CZTS (thin-film)	11.0 ± 0.2	0.2339(da)	0.7306	21.74 ^k	69.3	NREL (3/17)	UNSW on glass ³⁸
<u>Cells (other)</u>							
Perovskite (thin-film)	25.7 ± 0.8 ^{n,o}	0.09597 (ap)	1.1790	25.80 ⁱ	84.6	Newport (11/21)	UNIST Ulsan ³⁹
Organic (thin-film)	18.2 ± 0.2 ^p	0.0322 (da)	0.8965	25.72 ^g	78.9	NREL (10/20)	SJTU Shanghai/ Beihang U.
Dye sensitised	12.25 ± 0.4 ^q	0.0963 (ap)	1.0203	15.17 ^d	79.1	Newport (8/19)	EPFL ⁴⁰

Abbreviations: (ap), aperture area; (da), designated illumination area; (t), total area; AIST, Japanese National Institute of Advanced Industrial Science and Technology; CIGSSe, CuInGaSSe; CZTS, Cu₂ZnSnS₄; CZTSSe, Cu₂ZnSnS_{4-y}Se_y; DS, directionally solidified (including mono cast and multicrystalline); FhG-ISE, Fraunhofer-Institut für Solare Energiesysteme; ISFH, Institute for Solar Energy Research, Hamelin; NREL, National Renewable Energy Laboratory; PERC, passivated emitter and rear cell.

^aSpectral response reported in Version 36 of these tables.

^bNot measured at an external laboratory.

^cSpectral response and current–voltage curves reported in Version 51 of these tables.

^dSpectral response and current–voltage curves reported in Version 55 of these tables.

^eSpectral response and current–voltage curve reported in Version 52 of these tables.

^fContacting: Front: 12BB, busbar resistance neglecting; Rear: fully metallized, full area contacting.

^gSpectral response and current–voltage curves reported in Version 57 of these tables.

^hContacting: Front: 0BB, grid resistance neglecting; Rear: 9BB, full area contacting, highly reflective chuck.

ⁱSpectral response and current–voltage curves reported in the present version of these tables.

^jContacting: Front: 9BB, busbar resistance neglecting contacting; Rear: 9BB, full area contacting, highly reflective chuck.

^kSpectral response and current–voltage curves reported in Version 50 of these tables.

^lSpectral response and current–voltage curve reported in Version 54 of these tables.

^mSpectral response and/or current–voltage curves reported in Version 46 of these tables.

ⁿStability not investigated. References²⁵ and²⁶ document stability of similar devices.

^oMeasured using 10-point IV sweep with constant voltage bias until current change rate <0.07%/min.

^pLong-term stability not investigated. Tanenbaum et al.²⁸ and Krebs²⁹ document stability of similar devices.

^qLong-term stability not investigated. Krašovec et al.²⁷ documents stability of similar devices.

TABLE 3 Confirmed multiple-junction terrestrial cell and submodule efficiencies measured under the global AM1.5 spectrum (1000 W/m²) at 25°C (IEC 60904-3: 2008 or ASTM G-173-03 global)

Classification	Efficiency (%)	Area (cm ²)	V _{oc} (V)	J _{sc} (mA/cm ²)	Fill factor (%)	Test centre (date)	Description
III-V multijunctions							
Five-junction cell (bonded)	38.8 ± 1.2	1.021 (ap)	4.767	9.564	85.2	NREL (7/13)	Spectrolab, 2-terminal
(2.17/1.68/1.40/.73 eV)							
InGaP/GaAs/InGaAs	37.9 ± 1.2	1.047 (ap)	3.065	14.27 ^a	86.7	AIST (2/13)	Sharp, 2 term. ⁴¹
GalnP/GaAs (monolithic)	32.8 ± 1.4	1.000 (ap)	2.568	14.56 ^b	87.7	NREL (9/17)	LG Electronics, 2 term.
Multijunctions with c-Si							
GaN/P/GaInAsP/Si (wafer bonded)	35.9 ± 1.3 ^c	3.987 (ap)	3.248	13.11 ^d	84.3	FhG-ISE (4/20)	Fraunhofer ISE, 2-term. ⁴²
GaN/P/GaAs/Si (mech. stack)	35.9 ± 0.5 ^c	1.002 (da)	2.52/0.681	13.6/11.0	87.5/78.5	NREL (2/17)	NREL/CSEM/EPFL, 4-term. ⁴³
GaN/P/GaAs/Si (monolithic)	25.9 ± 0.9 ^c	3.987 (ap)	2.647	12.21 ^e	80.2	FhG-ISE (6/20)	Fraunhofer ISE, 2-term. ⁴⁴
GaAsP/Si (monolithic)	23.4 ± 0.3	1.026 (ap)	1.732	17.34 ^f	77.7	NREL (5/20)	OSU/UNSW/SolAero, 2-term ⁴⁵
GaAs/Si (mech. stack)	32.8 ± 0.5 ^c	1.003 (da)	1.09/0.683	28.9/11.1 ^g	85.0/79.2	NREL (12/16)	NREL/CSEM/EPFL, 4-term. ⁴³
Perovskite/Si (2-terminal)	29.8 ± 0.8 ^h	1.016 (da)	1.9193	19.45 ⁱ	79.8	FhG-ISE (11/21)	HZB, 2-term. ⁴⁶
GaN/P/GaInAs/Ge; Si (spectral split minimodule)	34.5 ± 2.0	27.83 (ap)	2.66/0.65	13.1/9.3	85.6/79.0	NREL (4/16)	UNSW/Azur/Trina, 4-term. ⁴⁶
Other multijunctions							
Perovskite/CIGS	24.2 ± 0.7 ^h	1.045 (da)	1.768	19.24 ^f	72.9	FhG-ISE (1/20)	HZB, 2-terminal ⁴⁷
Perovskite/perovskite	26.4 ± 0.7 ^{h,p}	1.044 (da)	2.118	15.22 ⁱ	82.6	JET (3/22)	SichuanU/EMPA, 2-term. ⁴⁹
Perovskite/perovskite (minimodule)	21.7 ± 0.6 ^h	20.25 (da)	2.009	14.22	75.9	JET (8/21)	Nanjing U, 2-term. ⁴⁸
a-Si/nc-Si/nc-Si (thin-film)	14.0 ± 0.4 ^{j,c}	1.045 (da)	1.922	9.94 ^k	73.4	AIST (5/16)	AIST, 2-term. ⁴⁹
a-Si/nc-Si (thin-film cell)	12.7 ± 0.4 ^{j,c}	1.000 (da)	1.342	13.45 ^l	70.2	AIST (10/14)	AIST, 2-term. ⁵⁰
'Notable exceptions'							
GaN/P/GaAs (mqw)	32.9 ± 0.5 ^c	0.250 (ap)	2.500	15.36 ^m	85.7	NREL (1/20)	NREL/UNSW, multiple QW
GaN/P/GaAs/GaInAs	37.8 ± 1.4	0.998 (ap)	3.013	14.60 ^m	85.8	NREL (1/18)	Microlink (ELO) ⁵¹
GaN/P/GaAs (mqw)/GaNAs	39.5 ± 0.5 ^c	0.242 (ap)	2.997	15.44 ⁿ	85.3	NREL (9/21)	NREL, multiple QW
Six-junction (monolithic) (2.19/1.76/1.45/1.19/.97/.7 eV)	39.2 ± 3.2 ^c	0.247 (ap)	5.549	8.457 ^o	83.5	NREL (11/18)	NREL, inv. metamorphic ⁵²
GaN/P/AlGaAs/CIGS	28.1 ± 1.2 ^c	0.1386 (da)	2.952	11.72 ^d	81.1	AIST (1/21)	AIST/FhG-ISE, 2-term. ⁵³
Perovskite/Si (large)	26.8 ± 1.2 ^h	274.22 (t)	1.891	17.84 ⁱ	79.4	FhG-ISE (11/21)	Oxford PV, 2-term.

(Continues)

TABLE 3 (Continued)

Classification	Efficiency (%)	Area (cm ²)	V _{oc} (V)	J _{sc} (mA/cm ²)	Fill factor (%)	Test centre (date)	Description
Perovskite/perovskite	28.0 ± 0.6 ^h	0.0495 (da)	2.125	16.42 ⁱ	80.3	JET (12/21)	Nanjing U, 2-term. ⁴⁸
Perovskite/organic	23.4 ± 0.8 ^h	0.0552 (da)	2.136	14.56 ⁱ	75.6	JET (3/22)	NUS/SERIS, 2-term. ⁵⁴

Abbreviations: (ap), aperture area; (da), designated illumination area; (t), total area; AIST, Japanese National Institute of Advanced Industrial Science and Technology; a-Si, amorphous silicon/hydrogen alloy; FhG-ISE, Fraunhofer Institut für Solare Energiesysteme; nc-Si, nanocrystalline or microcrystalline silicon.

^aSpectral response and current–voltage curve reported in Version 42 of these tables.

^bSpectral response and current–voltage curve reported in the Version 51 of these tables.

^cNot measured at an external laboratory.

^dSpectral response and current–voltage curve reported in Version 58 of these tables.

^eSpectral response and current–voltage curve reported in Version 57 of these tables.

^fSpectral response and current–voltage curve reported in Version 56 of these tables.

^gSpectral response and current–voltage curve reported in Version 52 of these tables.

^hInitial efficiency. References^{36,37} review the stability of similar perovskite-based devices.

ⁱSpectral response and current–voltage curves reported in the present version of these tables.

^jStabilised by 1000-h exposure to 1 sun light at 50°C.

^kSpectral response and current–voltage curve reported in Version 49 of these tables.

^lSpectral responses and current–voltage curve reported in Version 45 of these tables.

^mSpectral response and current–voltage curve reported in Version 53 of these tables.

ⁿSpectral response and current–voltage curves reported in Version 59 of these tables.

^oSpectral response and current–voltage curve reported in Version 54 of these tables. ^p

^pContacting: Front:3BB, busbar resistance neglecting; Rear: 3BB, full area contacting, high reflecting chuck.

TABLE 4 Confirmed non-concentrating terrestrial module efficiencies measured under the global AM1.5 spectrum (1000 W/m²) at a cell temperature of 25°C (IEC 60904-3: 2008 or ASTM G-173-03 global)

Classification	Effic. (%)	Area (cm ²)	V _{oc} (V)	I _{sc} (A)	FF (%)	Test centre (date)	Description
Si (crystalline)	24.4 ± 0.5	13,177 (da)	79.5	5.04 ^a	80.1	AIST (9/16)	Kaneka (108 cells) ⁴
Si (multicrystalline)	20.4 ± 0.3	14,818 (ap)	39.90	9.833 ^b	77.2	FhG-ISE (10/19)	Hanwha Q Cells (60 cells) ⁵⁵
GaAs (thin-film)	25.1 ± 0.8	866.45 (ap)	11.08	2.303 ^c	85.3	FhG-ISE (11/17)	Alta Devices ⁵⁶
CIGS (Cd-free)	19.2 ± 0.5	841 (ap)	48.0	0.456 ^c	73.7	AIST (1/17)	Solar Frontier (70 cells) ⁵⁷
CdTe (thin-film)	19.5 ± 0.3	23,582 (da)	227.9	2.622 ^d	76.9	NREL (9/21)	First Solar ⁵⁹
a-Si/nc-Si (tandem)	12.3 ± 0.3 ^e	14,322 (t)	280.1	0.902 ^f	69.9	ESTI (9/14)	TEL Solar, Trubbach Labs ⁵⁹
Perovskite	17.9 ± 0.5 ^g	804 (da)	58.7	0.323 ^h	76.1	AIST (1/20)	Panasonic (55 cells) ⁶⁰
Organic	8.7 ± 0.3 ⁱ	802 (da)	17.47	0.569 ^j	70.4	AIST (5/14)	Toshiba ⁶¹
<u>Multijunction</u>							
InGaP/GaAs/InGaAs	32.65 ± 0.7	965 (da)	24.30	1.520 ^d	85.3	AIST (2/223)	Sharp (40 cells; 8 series) ⁶³
<u>'Notable exception'</u>							
CIGS (large)	18.6 ± 0.6	10,858 (ap)	58.00	4.545 ^b	76.8	FhG-ISE (10/19)	Miasole ⁶³

Abbreviations: (ap), aperture area; (da), designated illumination area; (t), total area; a-Si, amorphous silicon/hydrogen alloy; a-SiGe, amorphous silicon/germanium/hydrogen alloy; CIGSS, CuInGaS_x; Effic., efficiency;

FF, fill factor; nc-Si, nanocrystalline or microcrystalline silicon.

^aSpectral response and current voltage curve reported in Version 49 of these tables.

^bSpectral response and current–voltage curve reported in Version 55 of these tables.

^cSpectral response and current–voltage curve reported in Version 50 or 51 of these tables.

^dSpectral response and current–voltage curve reported in the present version of these tables.

^eStabilised at the manufacturer to the 2% level following IEC procedure of repeated measurements.

^fSpectral response and/or current–voltage curve reported in Version 46 of these tables.

^gInitial performance. Han et al.²⁵ and Yang and You²⁶ review the stability of similar devices.

^hSpectral response and current–voltage curve reported in Version 57 of these tables.

ⁱInitial performance. Tanenbaum et al.²⁸ and Krebs²⁹ review the stability of similar devices.

^jSpectral response and current–voltage curve reported in Version 45 of these tables.

TABLE 5 Terrestrial concentrator cell and module efficiencies measured under the ASTM G-173-03 direct beam AM1.5 spectrum at a cell temperature of 25°C (except where noted for the hybrid and luminescent modules)

Classification	Effic. (%)	Area (cm ²)	Intensity ^a (suns)	Test centre (date)	Description
<u>Single cells</u>					
GaAs	30.8 ± 1.9 ^{b,c}	0.0990 (da)	61	NREL (1/22)	NREL, one junction (1J)
Si	27.6 ± 1.2 ^d	1.00 (da)	92	FhG-ISE (11/04)	Amonix back-contact ⁶⁴
CIGS (thin-film)	23.3 ± 1.2 ^{b,e}	0.09902 (ap)	15	NREL (3/14)	NREL ⁶⁵
<u>Multijunction cells</u>					
AlGaInP/AlGaAs/GaAs/GaInAs(3) (2.15/1.72/1.41/1.17/0.96/0.70 eV)	47.1 ± 2.6 ^{b,f}	0.099 (da)	143	NREL (3/19)	NREL, 6-J inv. metamorphic ⁵²
GalnP/GaAs; GaInAsP/GaInAs	46.0 ± 2.2 ^g	0.0520 (da)	508	AIST (10/14)	Soitec/CEA/FhG-ISE 4-J bonded ⁶⁶
GalnP/GaAs/GaInAs/GaInAs	45.7 ± 2.3 ^{b,h}	0.09709 (da)	234	NREL (9/14)	NREL, 4-J monolithic ⁶⁷
InGaP/GaAs/InGaAs	44.4 ± 2.6 ⁱ	0.1652 (da)	302	FhG-ISE (4/13)	Sharp, 3-J inverted metamorphic ⁶⁸
GalnAsP/GaInAs	35.5 ± 1.2 ^{b,j}	0.10031 (da)	38	NREL (10/17)	NREL two-junction (2J) ⁶⁹
<u>Minimodule</u>					
GalnP/GaAs; GaInAsP/GaInAs	43.4 ± 2.4 ^{b,k}	18.2 (ap)	340 ^l	FhG-ISE (7/15)	Fraunhofer ISE 4J (lens/cell) ⁷⁰
<u>Submodule</u>					
GalnP/GaInAs/Ge; Si	40.6 ± 2.0 ^k	287 (ap)	365	NREL (4/16)	UNSW 4-J split spectrum ⁷¹
<u>Modules</u>					
Si	20.5 ± 0.8 ^b	1875 (ap)	79	Sandia (4/89) ^l	Sandia/UNSW/ENTECH (12 cells) ⁷²
Three junctions (3J)	35.9 ± 1.8 ^m	1,092 (ap)	N/A	NREL (8/13)	Amonix ⁷³
Four junctions (4J)	38.9 ± 2.5 ⁿ	812.3 (ap)	333	FhG-ISE (4/15)	Soitec ⁷⁴
<u>Hybrid module^o</u>					
Four-junction (4J)/bifacial c-Si	34.2 ± 1.9 ^{b,o}	1,088 (ap)	CPV/PV	FhG-ISE (9/19)	FhG-ISE (48/8 cells; 4 T) ⁷⁵
<u>'Notable exceptions'</u>					
Si (large area)	21.7 ± 0.7	20.0 (da)	11	Sandia (9/90) ^l	UNSW laser grooved ⁷⁶
Luminescent minimodule ^o	7.1 ± 0.2	25 (ap)	2.5 ^p	ESTI (9/08)	ECN Petten, GaAs cells ⁷⁷
4J minimodule	41.4 ± 2.6 ^b	121.8 (ap)	230	FhG-ISE (9/18)	FhG-ISE, 10 cells ⁷⁰

Note: Following the normal convention, efficiencies calculated under this direct beam spectrum neglect the diffuse sunlight component that would accompany this direct spectrum. These direct beam efficiencies need to be multiplied by a factor estimated as 0.8746 to convert to thermodynamic efficiencies.

Abbreviations: (ap), aperture area; (da), designated illumination area; CIGS, CuInGaSe₂; Effic., efficiency; FhG-ISE, Fraunhofer-Institut für Solare Energiesysteme; NREL, National Renewable Energy Laboratory.

^aOne sun corresponds to direct irradiance of 1000 W m⁻².

^bNot measured at an external laboratory.

^cSpectral response and current–voltage curve reported in present version of these tables.

^dMeasured under a low aerosol optical depth spectrum similar to ASTM G-173-03 direct.⁷⁸

^eSpectral response and current–voltage curve reported in Version 44 of these tables.

^fSpectral response and current–voltage curve reported in Version 54 of these tables.

^gSpectral response and current–voltage curve reported in Version 45 of these tables.

^hSpectral response and current–voltage curve reported in Version 46 of these tables.

ⁱSpectral response and current–voltage curve reported in Version 42 of these tables.

^jSpectral response and current–voltage curve reported in Version 51 of these tables.

^kDetermined at IEC 62670-1 CSTC reference conditions.

^lRecalibrated from original measurement.

^mReferenced to 1000 W/m² direct irradiance and 25°C cell temperature using the prevailing solar spectrum and an in-house procedure for temperature translation.

ⁿMeasured under IEC 62670-1 reference conditions following the current IEC power rating draft 62670-3.

^oThermodynamic efficiency. Hybrid and luminescent modules measured under the ASTM G-173-03 or IEC 60904-3: 2008 global AM1.5 spectrum at a cell temperature of 25°C. 4-terminal module with external dual-axis tracking. Power rating of CPV follows IEC 62670-3 standard, front power rating of flat plate PV based on IEC 60904-3, -5, -7, -10 and 60891 with modified current translation approach; rear power rating of flat plate PV based on IEC TS 60904-1-2 and 60891.

^pGeometric concentration.

outright records, with solar cell efficiency targets in governmental research programmes generally specified in terms of a cell area of 1cm^2 or larger.^{79–81}

There are five new results reported in Table 3 relating to one-sun, multijunction devices, all involving a perovskite solar cell in various combinations, demonstrating the strength of this technology but also introducing concerns re long-term stability and toxicity. The first of these new results is 29.8% efficiency for a 1-cm^2 perovskite/silicon monolithic two-junction, two-terminal device fabricated by Helmholtz Centrum Berlin (HZB) and measured by the Fraunhofer Institute for Solar Energy Systems (FhG-ISE). The second is 26.4% efficiency measured for a 1-cm^2 perovskite/perovskite two-junction, two-terminal device fabricated by Sichuan University and EMPA, the Swiss Federal Laboratories for Materials Science and Technology, and measured by JET. The efficiency is 17% higher than the highest efficiency single-junction perovskite cell of similar size in Table 1 (smaller area cells in Table 2 have their efficiency inflated by avoiding series resistance and other compromises normally present in practical devices).

The three remaining new results in Table 3 appear as ‘notable exceptions’. The first is a landmark result of 26.8% for a large-area (274-cm^2) perovskite/silicon monolithic two-junction, two-terminal device fabricated by Oxford PV and measured by FhG-ISE. This result is notable since comparable in area and higher in efficiency than any single junction silicon cell. The second is a remarkable 28.0% efficiency measured for a small-area (0.05-cm^2) perovskite/perovskite two-junction, two-terminal device fabricated by Nanjing University⁴⁸ and measured by JET. The final new multijunction result is 23.4% for a small-area (0.06-cm^2) perovskite/organic two-junction, two-terminal device fabricated by the National University of Singapore (NUS) and the Solar Energy Research Institute of Singapore (SERIS)⁵⁴ and again measured by JET. The areas of the latter two devices are far too small for classification as outright records.

There are two new results for Table 4 (one-sun modules). The first is 19.5% efficiency for a large (2.4-m^2) CdTe module manufactured by First Solar⁵⁸ and measured by NREL. The second is 32.65% for a smaller area (965-cm^2) module using III-V triple-junction cells manufactured by Sharp⁶² and measured by the

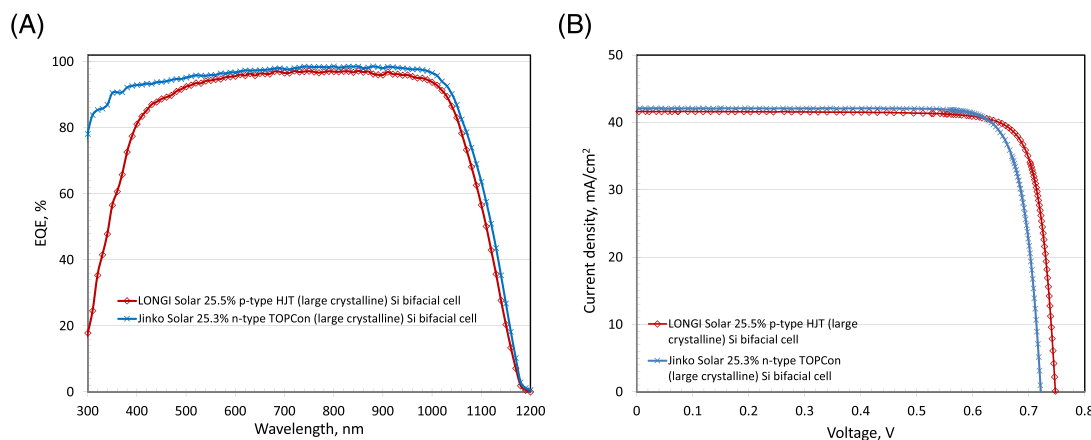


FIGURE 1 (A) External quantum efficiency (EQE) for the new Si cell results reported in this issue, (B) corresponding current density–voltage (JV) curves

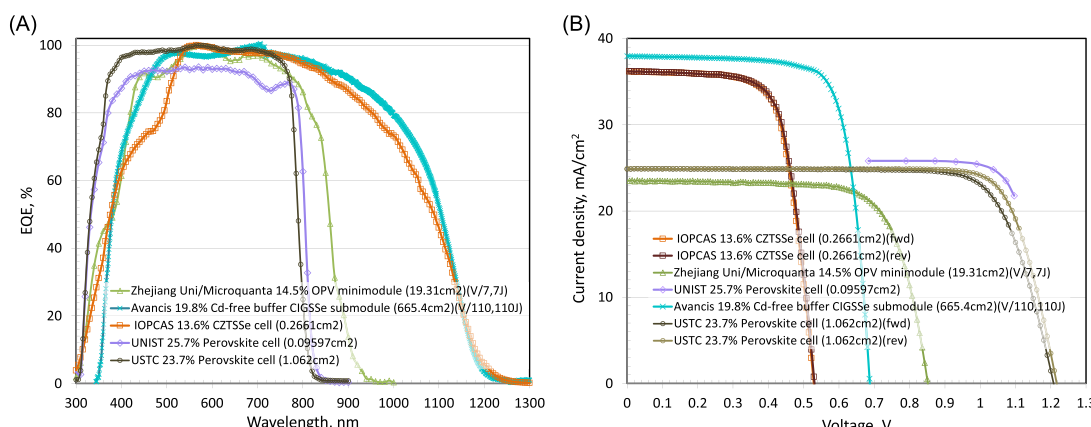


FIGURE 2 (A) External quantum efficiency (EQE) for the new thin-film cell and minimodule results reported in this issue (some results are normalised), (B) corresponding current density–voltage (JV) curves

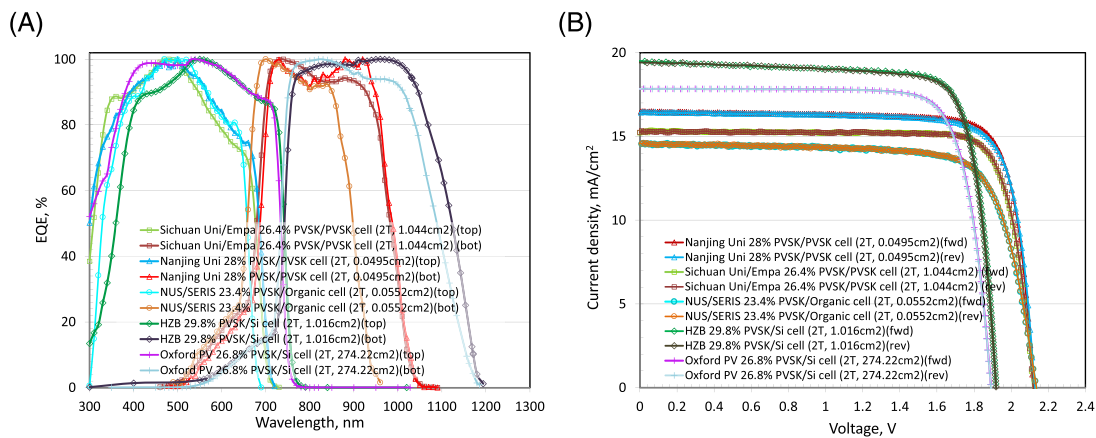


FIGURE 3 (A) External quantum efficiency (EQE) for the new multijunction cell results reported in this issue (all results are normalised), (B) corresponding current density–voltage (JV) curves

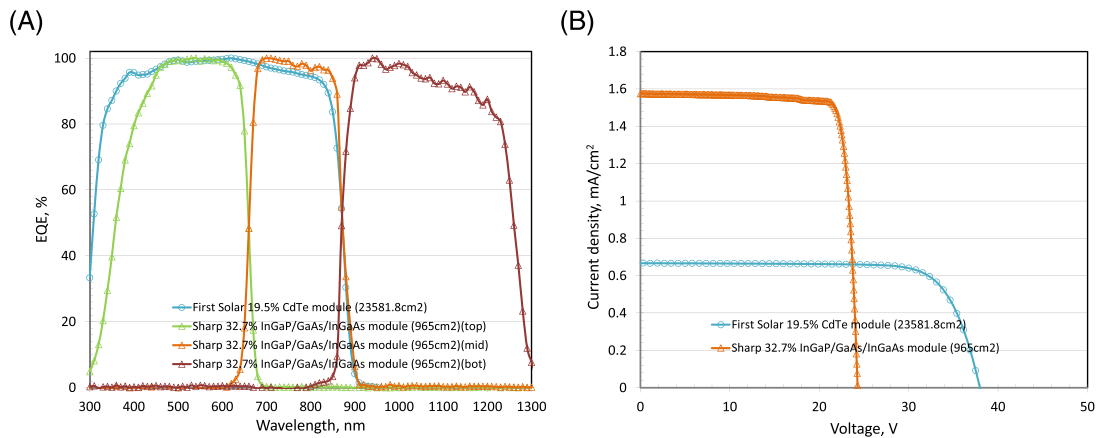


FIGURE 4 (A) External quantum efficiency (EQE) for the new module results reported in this issue (all results are normalised), (B) corresponding current density–voltage (JV) curves

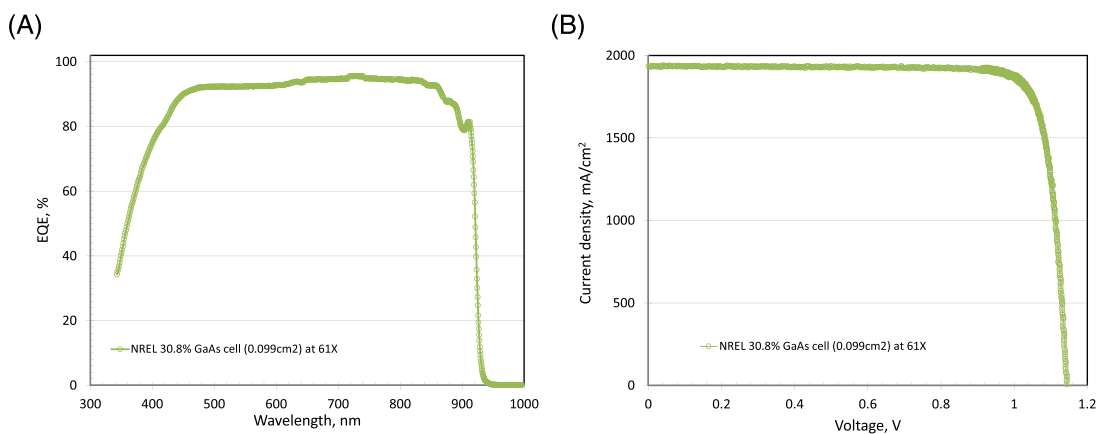


FIGURE 5 (A) External quantum efficiency (EQE) for the new GaAs concentrator cell result reported in this issue, (B) corresponding current density–voltage (JV) curve

Japanese National Institute of Advanced Industrial Science and Technology (AIST). This is a new outright record for a one-sun module, although slightly lower than that for a similar area flat-plate/concentrator hybrid module listed in Table 5 that requires more complex 4-terminal connection and accurate sun-tracking to operate efficiently.

The final result is in Table 5 (concentrator cells and modules) and documents an improvement to 30.8% efficiency for a single-junction GaAs concentrator cell fabricated and measured by NREL.

The EQE spectra for the new silicon cells reported in the present issue of these Tables are shown in Figure 1A, with Figure 1B showing the current density–voltage (JV) curves for the same devices. Figure 2A,B shows the corresponding EQE and JV curves for the new thin-film cell minimodule results, Figure 3A,B shows these for the new multijunction cell results, Figure 4A,B shows these for the new module results, while Figure 5A,B shows these for the new GaAs concentrator cell result.

ACKNOWLEDGEMENTS

The Australian Centre for Advanced Photovoltaics commenced operation in February 2013 with support from the Australian Government through the Australian Renewable Energy Agency (ARENA). The Australian Government does not accept responsibility for the views, information or advice expressed herein. The work at NREL was supported by the U.S. Department of Energy under Contract No. DE-AC36-08-GO28308 with the National Renewable Energy Laboratory. The work at AIST was supported in part by the Japanese New Energy and Industrial Technology Development Organisation (NEDO) under the Ministry of Economy, Trade and Industry (METI). Open access publishing facilitated by University of New South Wales, as part of the Wiley - University of New South Wales agreement via the Council of Australian University Librarians.

CONFLICT OF INTEREST

Although the information provided in the tables is provided in good faith, the authors, editors and publishers cannot accept direct responsibility for any errors or omissions.

DATA AVAILABILITY STATEMENT

The data that support the findings of this study are available from the corresponding author upon reasonable request.

ORCID

Martin A. Green  <https://orcid.org/0000-0002-8860-396X>
Michael Rauer  <https://orcid.org/0000-0002-4150-6150>

REFERENCES

- Green MA, Dunlop ED, Hohl-Ebinger J, Yoshita M, Kopidakis N, Hao XJ. Solar cell efficiency tables (Version 59). *Prog Photovolt: Res Appl.* 2022;30(1):3-12. doi:[10.1002/pip.3506](https://doi.org/10.1002/pip.3506)
- Green MA, Emery K, Hishikawa Y, Warta W. Solar cell efficiency tables (Version 33). *Prog Photovolt: Res Appl.* 2009;17(1):85-94. doi:[10.1002/pip.880](https://doi.org/10.1002/pip.880)
- Green MA, Dunlop ED, Hohl-Ebinger J, Yoshita M, Kopidakis N, Hao XJ. Solar cell efficiency tables (Version 57). *Prog Photovolt: Res Appl.* 2021;29(1):3-15. doi:[10.1002/pip.3371](https://doi.org/10.1002/pip.3371)
- Yoshikawa K, Kawasaki H, Yoshida W, et al. Silicon heterojunction solar cell with interdigitated back contacts for a photoconversion efficiency over 26%. *Nat Energy.* 2017;2(5):17032. doi:[10.1038/nenergy.2017.32](https://doi.org/10.1038/nenergy.2017.32)
- LONGi breaks three more world records for solar cell efficiency. 2021. https://en.longi-solar.com/home/events/press_detail/id/335.html
- Moslehi MM, Kapur P, Kramer J, et al. World-record 20.6% efficiency 156 mm × 156 mm full-square solar cells using low-cost kerfless ultrathin epitaxial silicon & porous silicon lift-off technology for industry-leading high-performance smart PV modules. *PV Asia Pacific Conference (APVIA/PVAP)*, 2012.
- Keevers MJ, Young TL, Schubert U, Green MA. 10% efficient CSG minimodules. 22nd European Photovoltaic Solar Energy Conference, Milan, 2007.
- Kayes BM, Nie H, Twist R, et al. 27.6% conversion efficiency, a new record for single-junction solar cells under 1 sun illumination. Proceedings of the 37th IEEE Photovoltaic Specialists Conference, 2011.
- Venkatasubramanian R, OQuinn BC, Hills JS, et al. 18.2% (AM1.5) efficient GaAs solar cell on optical-grade polycrystalline Ge substrate. Conference Record, 25th IEEE Photovoltaic Specialists Conference, Washington, 1997, 31-36.
- Wanlass M. Systems and methods for advanced ultra-high-performance InP solar cells. US Patent 9590131 B2, 2017.
- Nakamura M, Yamaguchi K, Kimoto Y, Yasaki Y, Kato T, Sugimoto H. Cd-free Cu (In,Ga)(Se,S)2 thin-film solar cell with a new world record efficacy of 23.35%. 46th IEEE PVSC. 2019 (see also http://www.solar-frontier.com/eng/news/2019/0117_press.html);9(6):1863-1867. doi:[10.1109/JPHOTOV.2019.2937218](https://doi.org/10.1109/JPHOTOV.2019.2937218)
- Diermann R. Avancis claims 19.64% efficiency for CIGS module. *PV Magazine International.* 2021;
- First Solar Press Release, First Solar builds the highest efficiency thin film PV cell on record, 2014.
- https://en.dgist.ac.kr/site/dgist_eng/menu/984.do (accessed 28 October 2018).
- Yan C, Huang J, Sun K, et al. Cu₂ZnSn S₄ solar cells with over 10% power conversion efficiency enabled by heterojunction heat treatment. *Nat Energy.* 2018;3(9):764-772. doi:[10.1038/s41560-018-0206-0](https://doi.org/10.1038/s41560-018-0206-0)
- Matsui T, Bidiville A, Sai H, et al. High-efficiency amorphous silicon solar cells: impact of deposition rate on metastability. *Appl Phys Lett.* 2015;106(5):053901. doi:[10.1063/1.4907001](https://doi.org/10.1063/1.4907001)
- Sai H, Matsui T, Kumagai H, Matsubara K. Thin-film microcrystalline silicon solar cells: 11.9% efficiency and beyond. *Appl Phys Express.* 2018;11(2):022301. doi:[10.7567/APEX.11.022301](https://doi.org/10.7567/APEX.11.022301)
- Xu JX, Boyd CC, Yu ZJ, et al. Triple-halide wide-band gap perovskites with suppressed phase segregation for efficient tandems, *Science.* 2020;367(6482):1097-1104. doi:[10.1126/science.aaz5074](https://doi.org/10.1126/science.aaz5074)
- <http://www.microquanta.com/en/>
- Han L, Fukui A, Chiba Y, et al. Integrated dye-sensitized solar cell module with conversion efficiency of 8.2%. *Appl Phys Lett.* 2009; 94(1):013305. doi:[10.1063/1.3054160](https://doi.org/10.1063/1.3054160)
- Komiya R, Fukui A, Murofushi N, Koide N, Yamanaka R, Katayama H. Improvement of the conversion efficiency of a monolithic type dye-sensitized solar cell module. Technical Digest, 21st International Photovoltaic Science and Engineering Conference, Fukuoka, 2011.
- Würfel U, Herterich J, List M, et al. A 1 cm² organic solar cell with 15.2% certified efficiency: detailed characterization and identification of optimization potential. *Sol RRL.* 2021;5(4):2000802. doi:[10.1002/solr.202000802](https://doi.org/10.1002/solr.202000802)

23. Fan JY, Liu ZX, Rao J, et al. High-performance organic solar modules via the bilayer-merged-annealing assisted blading coating. *Adv Mater.* 2022;2110569. doi:[10.1002/adma.202110569](https://doi.org/10.1002/adma.202110569)
24. https://www.enecn.de/fileadmin/user_upload/PR_opv-record_.pdf (accessed 11 November, 2019).
25. Han Y, Meyer S, Dkhissi Y, et al. Degradation observations of encapsulated planar $\text{CH}_3\text{NH}_3\text{PbI}_3$ perovskite solar cells at high temperatures and humidity. *J Mater Chem A.* 2015;3(15):8139-8147. doi:[10.1039/C5TA00358J](https://doi.org/10.1039/C5TA00358J)
26. Yang Y, You J. Make perovskite solar cells stable. *Nature.* 2017; 544(7649):155-156. doi:[10.1038/544155a](https://doi.org/10.1038/544155a)
27. Krašovec UO, Bokalič M, Topič M. Ageing of DSSC studied by electroluminescence and transmission imaging. *Sol Energy Mater Sol Cells.* 2013;117:67-72. doi:[10.1016/j.solmat.2013.05.029](https://doi.org/10.1016/j.solmat.2013.05.029)
28. Tanenbaum DM, Hermenau M, Voroshazi E, et al. The ISOS-3 inter-laboratory collaboration focused on the stability of a variety of organic photovoltaic devices. *RSC Adv.* 2012;2(3):882-893. doi:[10.1039/C1RA00686J](https://doi.org/10.1039/C1RA00686J)
29. Krebs FC. *Stability and Degradation of Organic and Polymer Solar Cells.* Chichester: Wiley; 2012; Jorgensen M, Norrman K, Gevorgyan SA, Tromholz T, Andreasen B, Krebs FC. Stability of polymer solar cells. *Advanced Materials* 2012; 24: 580-612. doi:[10.1002/adma.201104187](https://doi.org/10.1002/adma.201104187).
30. Green MA. The passivated emitter and rear cell (PERC): From conception to mass production. *Sol Energy Mater Sol Cells.* 2015;143:190-197. doi:[10.1016/j.solmat.2015.06.055](https://doi.org/10.1016/j.solmat.2015.06.055)
31. Richter A, Benick J, Feldmann F, Fell A, Hermle M, Glunz SW. n-Type Si solar cells with passivating electron contact: identifying sources for efficiency limitations by wafer thickness and resistivity variation. *Sol Energy Mater Sol Cells.* 2017;173:96-105. doi:[10.1016/j.solmat.2017.05.042](https://doi.org/10.1016/j.solmat.2017.05.042)
32. Haase F, Klamt C, Schäfer S, et al. Laser contact openings for local poly-Si-metal contacts enabling 26.1%-efficient POLO-IBC solar cells. *Sol Energy Mater Sol Cells.* 2018;186:184-193. doi:[10.1016/j.solmat.2018.06.020](https://doi.org/10.1016/j.solmat.2018.06.020)
33. Wang Q. Status of crystalline silicon PERC solar cells. NIST/UL Workshop on Photovoltaic Materials Durability, Gaithersburg, MD USA, 2019. doi:[10.17925/HI.2019.13.1.15](https://doi.org/10.17925/HI.2019.13.1.15).
34. <https://taiyangnews.info/technology/jinkosolar-record-25-25-efficiency-for-n-type-mono-cell/>
35. NREL. private communication, 2019.
36. First Solar Press Release. First Solar Achieves yet another cell conversion efficiency world record, 2016.
37. https://english.cas.cn/newsroom/research_news/phys/202203/t20220303_301861.shtml
38. Sun K, Yan C, Liu F, et al. Beyond 9% efficient kesterite $\text{Cu}_2\text{ZnSnS}_4$ solar cell: fabricated by using $\text{Zn}_{1-x}\text{Cd}_x\text{S}$ buffer layer. *Adv Energy Mater.* 2016;6(12):1600046. doi:[10.1002/aenm.201600046](https://doi.org/10.1002/aenm.201600046)
39. Jeong M, Choi IW, Go EM, et al. Stable perovskite solar cells with efficiency exceeding 24.8% and 0.3-V voltage loss. *Science.* 2020; 369(6511):1615-1620. doi:[10.1126/science.abb7167](https://doi.org/10.1126/science.abb7167)
40. <https://www.epfl.ch/labs/lspm/>; <https://www.epfl.ch/labs/lpi/> (accessed 28 October 2019).
41. Sasaki K, Agui T, Nakaido K, Takahashi N, Onitsuka R, Takamoto T. Proceedings, 9th International Conference on Concentrating Photovoltaics Systems, Miyazaki, Japan, 2013.
42. Müller R, Schygulla P, Lackner D, et al. Silicon-based monolithic triple-junction solar cells with conversion efficiency >34%. 37th European Photovoltaic Solar Energy Conference and Exhibition. 574-578. doi:[10.4229/EUPVSEC202020-3AO.7.2](https://doi.org/10.4229/EUPVSEC202020-3AO.7.2)
43. Essig S, Allezé C, Remo T, et al. Raising the one-sun conversion efficiency of III-V/Si solar cells to 32.8% for two junctions and 35.9% for three junctions. *Nat Energy.* 2017;2(9):17144. doi:[10.1038/nenergy.2017.144](https://doi.org/10.1038/nenergy.2017.144)
44. Feifel M, Lackner D, Schön J, et al. Epitaxial $\text{GaInP}/\text{GaAs}/\text{Si}$ triple-junction solar cell with 25.9% AM1.5g efficiency enabled by transparent metamorphic $\text{Al}_x\text{Ga}_{1-x}\text{As}_y\text{P}_{1-y}$ step-graded buffer structures. *Sol RRL.* 2021;5:2000763. doi:[10.1002/solr.202000763](https://doi.org/10.1002/solr.202000763)
45. Grassman TJ, Chmielewski DJ, Carnevale SD, Carlin JA, Ringel SA. $\text{GaAs}_{0.75}\text{P}_{0.25}/\text{Si}$ dual-junction solar cells grown by MBE and MOCVD. *IEEE J Photovolt.* 2016;6(1):326-331. doi:[10.1109/JPHOTOV.2015.2493365](https://doi.org/10.1109/JPHOTOV.2015.2493365)
46. Green MA, Keevers MJ, Concha Ramon B, et al. Improvements in sunlight to electricity conversion efficiency: above 40% for direct sunlight and over 30% for global. Paper 1AP.1.2, European Photovoltaic Solar Energy Conference 2015, Hamburg, 2015.
47. <https://www.pv-magazine.com/2019/09/11/hzb-hits-23-26-efficiency-with-cigs-perovskite-tandem-cell/> (accessed 28 October 2019).
48. Lin R, Xiao K, Qin ZY, et al. Monolithic all-perovskite tandem solar cells with 24.8% efficiency exploiting comproportionation to suppress Sn (II) oxidation in precursor ink. *Nat Energy.* 2019;4(10):864-873. doi:[10.1038/s41560-019-0466-3](https://doi.org/10.1038/s41560-019-0466-3)
49. Sai H, Matsui T, Koida T, Matsubara K. Stabilized 14.0%-efficient triple-junction thin-film silicon solar cell. *Appl Phys Lett.* 2016;109: 183506. doi:[10.1063/1.49669986](https://doi.org/10.1063/1.49669986)
50. Matsui T, Maejima K, Bidiville A, et al. High-efficiency thin-film silicon solar cells realized by integrating stable a-Si:H absorbers into improved device design. *Jpn J Appl Phys.* 2015;54(8S1):08KB10. doi:[10.7567/JJAP.54.08KB10](https://doi.org/10.7567/JJAP.54.08KB10)
51. <http://mldevices.com/index.php/news/> (accessed 28 October 2018).
52. Geisz JF, Steiner MA, Jain N, et al. Building a six-junction inverted metamorphic concentrator solar cell. *IEEE J Photovolt.* 2018;8(2):626-632. doi:[10.1109/JPHOTOV.2017.2778567](https://doi.org/10.1109/JPHOTOV.2017.2778567)
53. Makita K, Kamikawa Y, Mizuno H, et al. III-V// $\text{Cu}_x\text{In}_{1-y}\text{Ga}_y\text{Se}_2$ multi-junction solar cells with 27.2% efficiency fabricated using modified smart stack technology with Pd nanoparticle array and adhesive material. *Prog Photovolt Res Appl.* 2021;29(8):887-898. doi:[10.1002/pip.3398](https://doi.org/10.1002/pip.3398)
54. Chen W, Zhu YD, Xiu JW, et al. Monolithic perovskite/organic tandem solar cells with 23.6% efficiency enabled by reduced voltage losses and optimized interconnecting layer. *Nat Energy.* 2022;7(3): 229-237. doi:[10.1038/s41560-021-00966-8](https://doi.org/10.1038/s41560-021-00966-8)
55. <https://www.hanwha-qcells.com> (accessed 28 October 2019).
56. Mattos LS, Scully SR, Syfu M, et al. New module efficiency record: 23.5% under 1-sun illumination using thin-film single-junction GaAs solar cells. Proceedings of the 38th IEEE Photovoltaic Specialists Conference, 2012.
57. Sugimoto H. High efficiency and large volume production of CIS-based modules. 40th IEEE Photovoltaic Specialists Conference, Denver, 2014.
58. <http://www.firstsolar.com/en-AU/-/media/First-Solar/Technical-Documents/Series-6-Datasheets/Series-6-Datasheet.ashx> (accessed 28 October 2019).
59. Cashmore JS, Apolloni M, Braga A, et al. Improved conversion efficiencies of thin-film silicon tandem (MICROMORPH™) photovoltaic modules. *Sol Energy Mater Sol Cells.* 2016;144:84-95. doi:[10.1016/j.solmat.2015.08.022](https://doi.org/10.1016/j.solmat.2015.08.022)
60. Higuchi H, Negami T. Largest highly efficient 203 x 203 mm² $\text{CH}_3\text{NH}_3\text{PbI}_3$ perovskite solar modules. *Jpn J Appl Phys.* 2018; 57(8S3):08RE11. doi:[10.7567/JJAP.57.08RE11](https://doi.org/10.7567/JJAP.57.08RE11)
61. Hosoya M, Oooka H, Nakao H, et al. Organic thin film photovoltaic modules. *Proceedings of the 93rd Annual Meeting of the Chemical Society of Japan.* 2013;21-37.
62. Takamoto T. Application of InGaP/GaAs/InGaAs triple junction solar cells to space use and concentrator photovoltaic. 40th IEEE Photovoltaic Specialists Conference, Denver, 2014.
63. Bheemreddy V, Liu BJJ, Wills A, Murcia CP. Life prediction model development for flexible photovoltaic modules using accelerated

- damp heat testing. *IEEE 7th World Conf. on Photovoltaic Energy Conversion (WCPEC)*. 2018;1249-1251.
64. Slade A, Garboushian V. 27.6% efficient silicon concentrator cell for mass production. Technical Digest, 15th International Photovoltaic Science and Engineering Conference, Shanghai, 2005.
 65. Ward JS, Ramanathan K, Hasoon FS, et al. A 21.5% efficient Cu (In,Ga)Se₂ thin-film concentrator solar cell. *Prog Photovolt: Res Appl*. 2002;10(1):41-46. doi:[10.1002/pip.424](https://doi.org/10.1002/pip.424)
 66. Dimroth F, Tibbets TND, Niemeyer M, et al. Four-junction wafer-bonded concentrator solar cells. *IEEE J Photovolt*. 2016;6(1):343-349. doi:[10.1109/JPHOTOV.2015.2501729](https://doi.org/10.1109/JPHOTOV.2015.2501729)
 67. NREL Press Release NR-4514, 2014.
 68. Press Release, Sharp Corporation, 2012 (accessed at <http://sharp-world.com/corporate/news/120531.html> on 5 June 2013).
 69. Jain N, Schulte KL, Geisz JF, et al. High-efficiency inverted metamorphic 1.7/1.1 eV GaInAsP/GaInAs dual-junction solar cells. *Appl Phys Lett*. 2018;112(5):053905. doi:[10.1063/1.5008517](https://doi.org/10.1063/1.5008517)
 70. Steiner M, Siefer G, Schmidt T, Wiesenfarth M, Dimroth F, Bett AW. 43% sunlight to electricity conversion efficiency using CPV. *IEEE J Photovolt*. 2016;6(4):1020-1024. doi:[10.1109/JPHOTOV.2016.2551460](https://doi.org/10.1109/JPHOTOV.2016.2551460)
 71. Green MA, Keevers MJ, Thomas I, Lasich JB, Emery K, King RR. 40% efficient sunlight to electricity conversion. *Prog Photovolt: Res Appl*. 2015;23(6):685-691. doi:[10.1002/pip.2612](https://doi.org/10.1002/pip.2612)
 72. Chiang CJ, Richards EH. A 20% efficient photovoltaic concentrator module. *Conf Record, 21st IEEE Photovoltaic Specialists Conference, Kissimmee*. 1990;861-863.
 73. <http://amonix.com/pressreleases/amonix-achieves-world-record-359-module-efficiency-rating-nrel-4> (accessed 23 October 2013).
 74. van Riesen S, Neubauer M, Boos A, et al. New module design with 4-junction solar cells for high efficiencies. Proceedings of the 11th Conference on Concentrator Photovoltaic Systems, 2015.
 75. Martínez JF, Steiner M, Wiesenfarth M, Siefer G, Glunz S W, Dimroth F. Power rating procedure of hybrid CPV/PV bifacial modules. *Prog Photovolt Res Appl*. 2021;29(6):614-629. doi:[10.1002/pip.3410](https://doi.org/10.1002/pip.3410)
 76. Zhang F, Wenham SR, Green MA. Large area, concentrator buried contact solar cells. *IEEE Trans Electron Dev*. 1995;42(1):144-149. doi:[10.1109/16.370024](https://doi.org/10.1109/16.370024)
 77. Slooff LH, Bende EE, Burgers AR, et al. A luminescent solar concentrator with 7.1% power conversion efficiency. *Phys Stat Sol (RRL)*. 2008;2(6):257-259. doi:[10.1002/pssr.200802186](https://doi.org/10.1002/pssr.200802186)
 78. Gueymard CA, Myers D, Emery K. Proposed reference irradiance spectra for solar energy systems testing. *Solar Energy*. 2002;73(6):443-467. doi:[10.1016/S0038-092X\(03\)00005-7](https://doi.org/10.1016/S0038-092X(03)00005-7)
 79. Photovoltaics, Solar Energy Research Institute, Program milestones and decision points for single junction thin films. Annual Progress Report 1984, Report DOE/CE-0128, 1985, 7.
 80. Sakata I, Tanaka Y, Koizawa K. Japans new national R&D program for photovoltaics. *Photovoltaic Energy Conversion, Conference Record of the 2006 IEEE 4th World Conference*. 2008;1:1-4.
 81. Jäger-Waldau A (Ed). *PVNET: European Roadmap for PV R&D*, EUR 21087 EN. Vol. 451-452; 2004:448-454. doi:[10.1016/j.tsf.2003.10.140](https://doi.org/10.1016/j.tsf.2003.10.140).
 82. Hohl-Ebinger J, Grote D, Hund B, Mette A, Warta W. Contacting bare solar cells for STC measurements. Proceedings of the 23rd European Photovoltaic Solar Energy Conference and Exhibition, Valencia, Spain, 2008, pp. 2012-2016.
 83. Geisemeyer I, Kallies C, Hohl-Ebinger J, Warta W. Contacting bare silicon solar cells with advanced cell metallisation. Proceedings of the 29th European Photovoltaic Solar Energy Conference and Exhibition, Amsterdam, The Netherlands, 2014, pp. 1202-1207.
 84. Kruse CN, Wolf M, Schincke C, Hinken D, Brendel R, Bothe K. Impact of contacting geometries on measured fill factors. *Energy Proc*. 2017;124:84-90. doi:[10.1016/j.egypro.2017.09.329](https://doi.org/10.1016/j.egypro.2017.09.329)
 85. Bothe K, Kruse C, Hinken D, Brendel R, Rauer M, Hohl-Ebinger J. Contacting of busbarless solar cells for accurate I-V measurements. *Proceedings of the 37th European Photovoltaic Solar Energy Conference and Exhibition, Online*, 2020, pp. 277-281.
 86. Rauer M, Krieg A, Pfreundt A, Mittag M, Pingel S. The challenge of measuring busbarless solar cells and the impact on cell-to-module losses. *Photovolt Int*. 2020;45:8-18.
 87. Rauer M, Bothe K, Comparotto C, et al. Monofacial IV measurements of bifacial solar cells in an Interlaboratory Comparison. *Proceedings of the 32nd European Photovoltaic Solar Energy Conference and Exhibition, Munich, Germany*, 2016, pp. 915-921.
 88. Shimura H, Sasaki A, Ohshima H, Hishikawa Y. Accurate performance evaluation of conventional and crystalline silicon solar cells. *Proceedings of 6th World Conference on Photovoltaic Energy Conversion, Kyoto*. 2014, pp. 10.

How to cite this article: Green MA, Dunlop ED, Hohl-Ebinger J, et al. Solar cell efficiency tables (Version 60). *Prog Photovolt Res Appl*. 2022;30(7):687-701. doi:[10.1002/pip.3595](https://doi.org/10.1002/pip.3595)

APPENDIX A: TEMPORARY ELECTRICAL CONTACTING OF LARGE-AREA SOLAR CELLS

Edited by: Karsten Bothe, ISFH, David Hinken, ISFH, Jochen Hohl-Ebinger, Fraunhofer ISE and Michael Rauer, Fraunhofer ISE.

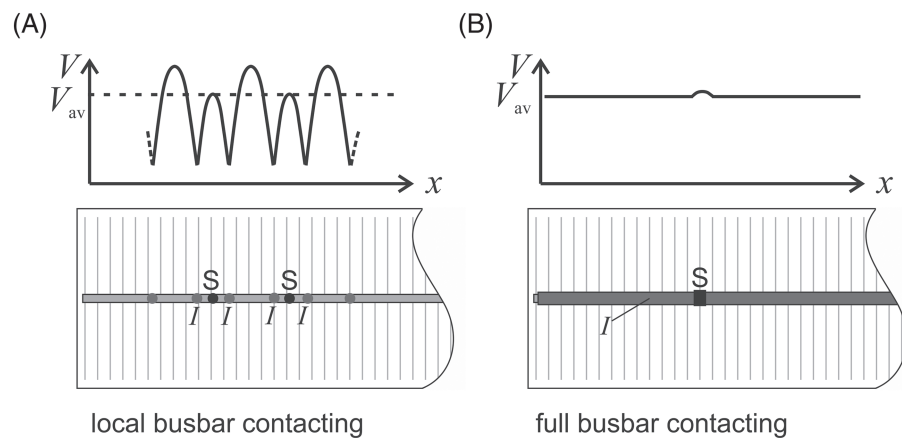
The temporary, non-destructive electrical contacting of bare solar cells is one of the greatest challenges for precise and correct measurements of the current-voltage characteristics and determination of the characteristic solar cell parameters. In recent years, this has become increasingly complex for large-area solar cells, as solar cell concepts and their metallization schemes have diversified considerably. Because there is no explicit standard for the design of solar cell contacting units, we describe approaches for temporary electrical contacting of large-area solar cells with and without busbars. Special attention is given to the voltage measurement also called sensing. In order to enable comparability between different contacting approaches and to bring structure to the corresponding measurement conditions, an unambiguous denotation is introduced.

A.1 | Contacting the solar cell front side

A.1.1 | Solar cells with busbars

For the measurement of solar cells with conventional H-pattern metallization, the generally accepted concept is an infinite number of current contact points on the busbars. Using this ideal contacting scheme, the resistance of the busbars becomes negligible. The energy conversion efficiency associated with this measurement is therefore called *busbar-resistance neglecting (brn)* efficiency. This is a widely

FIGURE A1 Two possible schemes for contacting the busbar of solar cells: (A) Local busbar contacting with smart positioning of the spring-loaded pins and (B) full busbar contacting using an elastic contacting bar with a narrow sense segment. The sense contact of both schemes measures the average busbar potential V_{av}



accepted approach in the whole photovoltaic community since many years. Note that the finger resistance impacts on the measured cell performance for this contacting approach.

Having only a finite number of current contacts, it was shown^{82–84} that a specific smart positioning of the voltage sense contacts allows to approximate the ideal contacting scheme and thereby provides the same efficiency and the same fill factor. Figure A1 illustrates two possible schemes for contacting the busbar of solar cells. Figure A1A shows local busbar contacting with spring-loaded pins and a smart positioning for the voltage sensing pin. Here, triplets of pins (current-sense-current) are exemplarily used; the sense pin measures the average potential V_{av} . Other smart positioning layouts are feasible.⁸⁴ Figure A1B shows the full busbar contacting using an elastic contacting bar with a narrow voltage sensing segment that also measures the average busbar potential V_{av} .

A.1.2 | Solar cells without busbars (BBO cells)

For BBO solar cells, two different contacting approaches exist.

The first approach transfers the ideal contacting concept of infinite contacting points on the busbar to infinite contacting points on the fingers. Consequently, with this idealised contacting scheme, the resistance of the fingers becomes negligible and the energy conversion efficiency associated with this measurement is called *grid-resistance neglecting (grn)* efficiency. This approach can be realised with a sufficiently high number of current contact bars or wires⁸⁵ or with specific smart positioning of the voltage measuring contact (sense contact) for a lower number of contact bars.^{85,86}

The second approach is to align the contacting system with the interconnection of the solar cell in the module and to use an equivalent number of contact bars or wires. In this case, the series resistance of the metal grid impacts on the measurement result leading to the so-called *grid-resistance including (gri)* energy conversion efficiency. As this impact of the metal grid critically depends on the number of current bars or wires, specifying this number (the position is assumed to be equidistant) is essential for this approach. For the contacting with 12 current contact bars, for example, the notation would be gri, 12CC.

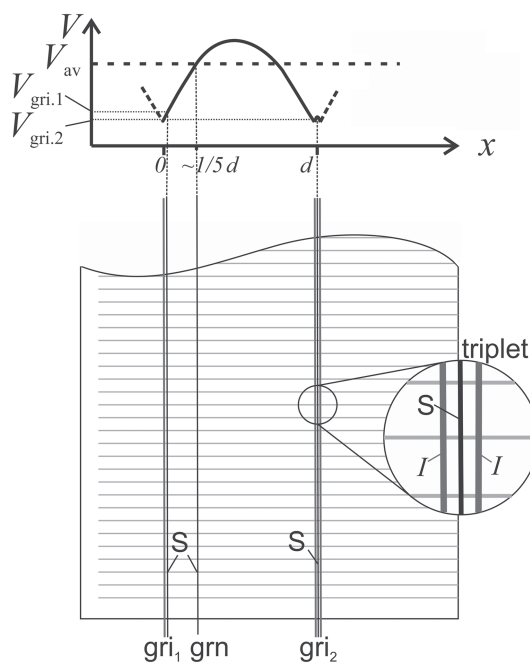


FIGURE A2 Contacting the fingers of a BBO solar cell by wires or suitable contacting bars. Sensing is carried out either with the grn approach (at a distance of 1/5th of the distance of two adjacent contacts) or with the gri approach (as close as possible to a current contact), which considers the series resistance of the metal grid

The technical realisation of the gri approach might be difficult, as any distance between voltage sense and adjacent current contact leads to an overestimation of the measured efficiency. The extent of overestimation depends on the actual distance between sense and current contact as well as on the finger resistance. A triplet configuration (current-sense-current) with very small distances might be a technical solution to reduce this overestimation.

Figure A2 illustrates both approaches. For the grn approach, the smart sensing is carried out at approximately 1/5th of the distance d of two adjacent contacts. This position provides the same efficiency as contacting the entire metallized area. Note that for very high finger resistances, the position might differ slightly. The larger the potential

distribution the larger the impact of a misplacement of the sensing contact. Other smart layouts are possible. In contrast, for the gri approach, the voltage sense has to be positioned very close to a current contact (gri_1). Alternatively, a current-sense-current triplet configuration (gri_2) can be used which reduces the risk of efficiency overestimation.

A.2 | Contacting the solar cells rear side

The metallization of the solar cell rear surface has changed significantly in recent years, especially for industrial solar cells. Full-surface rear metallization has been standard for many years (monofacial solar cells), which is denoted as *fully metallized (fm)* here. Today, most solar cells exhibit a local rear contact grid similar to front side metallization, which either includes busbars or is busbarless. These bifacial solar cells are sensitive to light on both sides.

Chucks made of metal electrically contact the entire rear metallization of the solar cells. For voltage measurement, these chucks often have an electrically insulated sense segment. This contacting scheme is referred to as *full-area contacting (fac)*. If bifacial cells are measured on such chucks, the entire rear fingers and the rear busbars are contacted and thus their resistivity is automatically neglected.

Alternatively, the rear of bifacial cells may be contacted only locally with a certain number of current contacts analogous to the contacting of the solar cell front side. The contacting scheme is then referred to as *local contacting (loc)*. Depending on the specific design of the solar cell metallization layout, the rear contacting scheme can then either be **brn**, **grn** or **gri**, in analogy to the definitions of the front contacting.

A.3 | Chuck reflectance

In addition to the conductivity of the measuring chucks, the reflectance of the chucks also affects the measurement result for bifacial solar cells, as some of the light incident on the front side

may be transmitted through the cell and reflected at the chuck surface.

If bifacial solar cells are measured on chucks made of highly reflective materials (e.g., brass) or on chucks coated with highly reflective metals (e.g., gold), the transmitted and reflected light results in additional illumination of the rear side of the solar cell. For typical solar cells, this can lead to an increase in short-circuit current I_{SC} of about 1.0%–1.5%.⁸⁷ For clarification, Figure A3A shows the transmittance of a bifacial passivated emitter and rear cell (PERC) solar cell (green line), the reflectance of a gold-coated chuck and of a non-reflective chuck (nrc). Figure A3B shows a typical solar simulator spectrum as well as the spectrum at the solar cell rear caused by the solar simulated irradiance reflected back from a gold-coated chuck after passing through the cell. To indicate this potential current gain in the efficiency tables, the short-circuit current of bifacial solar cells measured on a highly reflective chuck (hrc) is marked as: measured on a hrc. Typical chuck reflectances are >85% in the relevant wavelength range (above 900 nm for Si solar cells).

Short-circuit currents measured on a nrc complying with the requirements of IEC TS 60904-1-2 bear the indication: measured on a nrc. To meet the requirements of this IEC TS, chuck reflectances <15% in the relevant wavelength range shall be used for today's solar cells. Alternatively, measurements on reflective chucks can be corrected for the light incident onto the rear,⁸⁸ which likewise leads to nrc conditions.

For monofacial solar cells, the chuck reflectance is not relevant, so that no further specification of the reflectance is needed.

A.4 | Summary of notations

In summary, we introduce new abbreviations to indicate additional conditions relevant for assessing efficiency measurements. For specifying the solar cell metallization, the numbers of busbars shall be stated for front and rear or the rear side shall be specified as fm.

For describing the contacting schemes, the following notation for front and rear side is introduced:

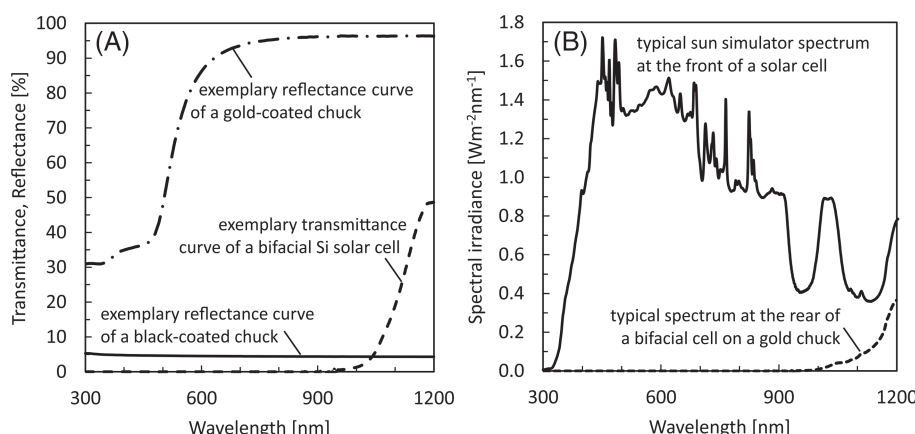


FIGURE A3 (A) Reflectance curves of a gold and a black-coated chuck as well as transmittance curve of a bifacial silicon solar cell, (B) spectral irradiance of a solar simulator at the front of a solar cell as well as spectral irradiance at the rear of a bifacial silicon solar cell caused by radiation from the sun simulator that is reflected back from a gold-coated chuck after passing through the bifacial cell

- busbar-resistance neglecting: **brn**
- grid-resistance neglecting: **grn**
- grid-resistance including: **gri** with specification of the number of current contacts
- full-area contacting: **fac**
- local contacting: **loc**

For the interpretation of the short-circuit current of bifacial cells, note the following conditions:

- highly reflective chuck: **hrc**
- non-reflective chuck: **nrc**

Examples:

1. A monofacial solar cell with 12 busbars on the front and fm rear is measured with electrical contact to the front busbars. Because the solar cell is monofacial, the rear contacting scheme and reflectance of the chuck are not relevant. The denotation for this measurement would be:
front: 12BB, brn; rear: fm, fac.
2. A bifacial solar cell with 12 busbars on the front and 12 busbars on the rear is measured with electrical contact to the front busbars on a nrc that contacts only the rear busbars. The denotation for this measurement would be the following:
front: 12BB, brn; rear: 12BB, loc, brn, nrc.
3. A bifacial solar cell without busbars on both front and rear is measured on an hrc. The front grid of the cell is contacted with a high number of current contact bars or by smart voltage sensing, the

rear grid is electrically fully contacted. The denotation for this measurement would be the following:
front: OBB, grn; rear: OBB, fac, hrc.

4. A monofacial solar cell without busbars on front and fm rear is measured with nine current contact bars on the front, voltage sensing is carried out with the grid resistance including approach. Because the solar cell is monofacial, the rear contacting scheme and reflectance of the chuck are not relevant. The denotation for this measurement would be the following:
front: OBB, gri, 9CC; rear: fm, fac.

APPENDIX B: LIST OF DESIGNATED TEST CENTRES

A list of designated test centres is contained in an earlier issue.³ One change:

Important note for Newport PV Lab customers:

All samples for measurement should be shipped to the new laboratory location at the following address:

Attn: PV Lab.
3050 North 300 West.
North Logan, UT 84341.
Contact: Jake Sorensen.
Email: jacob.sorensen@mksinst.com
Main: +435-753-3729.
Fax: +435-753-5231.
(Terrestrial cells)